Diffusion-tensor (DT) imaging is a magnetic resonance (MR) imaging technique that is sensitive to the orientation of mobility in intravoxel water molecules (1,2). DT imaging reveals two specific characteristics: diffusion anisotropy and the directional distribution of water diffusivity. When water diffusion in a tissue is almost the same in all directions, the diffusion is considered to be isotropic and have lower anisotropy. Conversely, when water diffusion is restricted along a specific direction, the diffusion is considered to be anisotropic and have higher anisotropy. Brain white matter has high diffusion anisotropy because diffusion is faster when it is parallel to the fiber direction than when it is the same in all other directions (3,4).

DT images of the human brain can be reconstructed for visualization of the macroscopic three-dimensional fiber tract architecture by using a process known as fiber tractography, or the fiber-tracking technique (5–10). DT imaging and fiber tractography are powerful tools for studying cerebral white matter and have been applied clinically to assess brain tumors (11,12), diffuse axonal injury (13), pediatric brain development (14), and cerebral infarcts (15).

With recent advances in actively shielded 3.0-T magnets, the use of high-field-strength MR imaging in clinical settings has become practical (16,17). Parallel imaging techniques, such as simultaneous acquisition of spatial harmonics, or SMASH (18); sensitivity encoding (19); and auto-SMASH–based generalized autocalibrating partially parallel acquisition (20), also have improved with recent advances in MR imaging hardware. Owing to shortened echo train lengths and echo times, parallel imaging techniques can be used to reduce artifacts related to spin-echo echo-planar imaging. Some reports have described the performance of parallel imaging in spin-echo echo-planar DT imaging and fiber tractography at 1.5 or 3.0 T (9,10,21–24). However, to our knowledge, in no reports have the differences between 3.0- and 1.5-T spin-echo echo-planar DT fiber tractography with parallel imaging been compared. Thus, the purpose of our study was to prospectively evaluate the depiction of brain fiber tracts at 3.0-T versus 1.5-T DT fiber tractography performed with parallel imaging.

Materials and Methods

Study Subjects

The study population comprised 30 healthy volunteers (15 men, 15 women; mean age, 28 years; age range, 21–46 years) with no history of neurologic injury or psychiatric disease. All subjects were examined by one of the authors (T.H., with 14 years of experience as a neurologist), and no subjects had abnormal neurologic signs or symptoms. Institutional review board approval was obtained for this study, and each subject provided written informed consent.

Data Acquisition

All subjects underwent 3.0- and 1.5-T DT imaging, which was performed by using a whole-body 3.0-T MR unit (Trio; Siemens, Erlangen, Germany) with a 40 mT/m gradient and a 1.5-T MR unit (Symphony; Siemens) with a 30 mT/m gradient, on the same day. MR imaging at 3.0 T was performed by one author (T.O.), and MR imaging at 1.5 T was performed by another author (Y.F.), both of whom had 8 years of experience as neuroradiologists and 2 years of experience in DT imaging. The time delay between 3.0- and 1.5-T MR imaging was less than 1 hour for all subjects. Both MR units were equipped with integrated parallel acquisition capability and a receive-only eight-channel phased-array head coil. Both the 3.0-T and the 1.5-T DT imaging examinations involved the use of single-shot spin-echo echo-planar sequences and nearly identical parameters: 5200/79 (repetition time msec/echo time msec), a 220-mm field of view, a 128 × 128 matrix, 3-mm section thickness without intersection gaps (matrix size, 1.7 × 1.7 × 3.0 mm), and four repetitions.

The generalized autocalibrating partially parallel acquisition algorithm was applied for parallel imaging with use of a reduction factor of two, 24 additional autocalibrating phase-encoding steps in the center of k-space, and a 75% partial Fourier technique in the phase-encoding direction. Only the bandwidths differed: A bandwidth of 1502 Hz per pixel was used for 3.0-T imaging, and a bandwidth of 1056 Hz per pixel was used for 1.5-T imaging. Motion-probing gradients were applied along 12 noncolinear directions with a b factor of 700 sec/mm^2 after one non–diffusion-weighted image (b = 0 sec/mm^2) was obtained. A total of 40 sections encompassed the entire cerebral hemisphere and the brainstem. The imaging times for 3.0- and 1.5-T DT imaging were almost the same—about 7.5 minutes.

Data Processing

DT imaging data sets were transferred, in Digital Imaging and Communications in Medicine format, to a Windows personal computer (IBM, New York, NY) workstation. DtiStudio, version 1.02, software (H. Jiang, S. Mori, Department of Radiology, Johns Hopkins University, Baltimore, Md) was used for tensor calculations (6,10). All source images from the DT imaging data sets were visually inspected by one author (T.O.), and images with visually apparent artifacts due to bulk motion were removed. In our DT imaging data set, there was low eddy current–related

Published online before print
10.1148/radiol.2382042192

Radiology 2006; 238:668–678

Abbreviations:
DT = diffusion tensor
ROI = region of interest

Author contributions:
Guarantors of integrity of entire study, T.O., Y.M., K.T.; study concepts/study design or data acquisition or data analysis/interpretation, all authors; manuscript drafting or manuscript revision for important intellectual content, all authors; approval of final version of submitted manuscript, all authors; literature research, T.O., Y.M., Y.F., H.F., M.H., K.T.; clinical studies, T.O., Y.M., Y.F., T.H., M.K., A.Y., S.U., K.T.; statistical analysis, T.O., Y.M., M.K., A.Y., M.H., K.T.; and manuscript editing, all authors

Address correspondence to Y.M. (e-mail: *mikiy@kuhp.kyoto-u.ac.jp*).

Authors stated no financial relationship to disclose.

geometric distortion between images obtained in each motion-probing gradient direction (23,25), so postprocessing distortion correction was not applied for this data set. After calculating the six independent elements of the 3 × 3 tensor and diagonalization, three eigenvalues and three eigenvectors were obtained (1,3–5). The eigenvector associated with the largest eigenvalue was assumed to represent the intravoxel fiber orientation. The fractional anisotropy map and directional color-coded map were synthesized (Fig 1). Fiber orientations were assigned specific colors on the color-coded map, as follows: Red represented the right-to-left orientation; green, the anterior-to-posterior orientation; and blue, the superior-to-inferior orientation (26).

Fiber Tractography

The DtiStudio software was used to also perform fiber tractography on the basis of the fiber assignments derived by means of the continuous tracking method (6,9,10). With this software, tracking from all the pixels inside the brain (ie, with the brute force approach) was performed, and tracking results that penetrated the two manually segmented regions of interest (ROIs) on the basis of the known anatomic distributions of tracts were assigned to specific tracts (ie, with the two-ROI approach). Propagation in each fiber tract was terminated if a voxel with a fractional anisotropy value of less than 0.2 was reached or if the inner product of two consecutive vectors was greater than 0.75. These conditions prohibited the turning of angles larger than 41° during tracking (10).

Four fiber bundles—the corticospinal tract, the superior longitudinal fasciculus, the corticocortical connection fibers through the corpus callosum, and the limbic fibers through the fornix—were reconstructed by drawing specific ROIs according to the anatomic distributions of each fiber tract. ROI manipulations were performed by one neuroradiologist (A.Y.) with 3 years of experience performing tractography and 10 years of experience as a neuroradiologist. This author was blinded as to whether the images had been obtained by using 3.0 T or 1.5 T when he performed each ROI segmentation.

For corticospinal tract tractography, two ROIs were placed on transverse non–diffusion-weighted (b = 0 sec/mm^2) images (10,12,15) according to established anatomic landmarks: The first ROI was placed in the cerebral peduncle bilaterally, and the second ROI was placed in the precentral gyrus bilaterally (27) (Fig 2a).

The superior longitudinal fasciculus was reconstructed at tractography by placing two ROIs in the cerebral deep white matter on a coronal directional color-coded map. The superior longitudinal fasciculus was identified on the coronal color-coded map as a region where the fiber orientation was anterior to posterior (green), lateral to the corona radiata (26,28). An anterior ROI was placed in the plane passing through the reconstructed corticospinal tract, and a posterior ROI was placed in the plane passing through the rostral surface of the splenium of the corpus callosum, with both ROIs covering the green area representing the superior longitudinal fasciculus (Fig 2c). Some "noise" fibers that were apparently tracing the error course were then removed (10).

Corpus callosum tractography was performed by imaging the combination of four different callosal fiber bundles. The primary ROI was placed in the corpus callosum in the midsagittal plane (Fig 2d). To visualize different parts of the callosal fibers, secondary ROIs were placed in four regions: two ROIs on the coronal color-coded map and two ROIs on the transverse color-coded map (Fig 2e). Anterior callosal fibers, referred to as minor forceps, were reconstructed by placing the ROI covering the deep white matter in the coronal plane anterior to the genu of the corpus callosum. For reconstruction of the posterior cal-

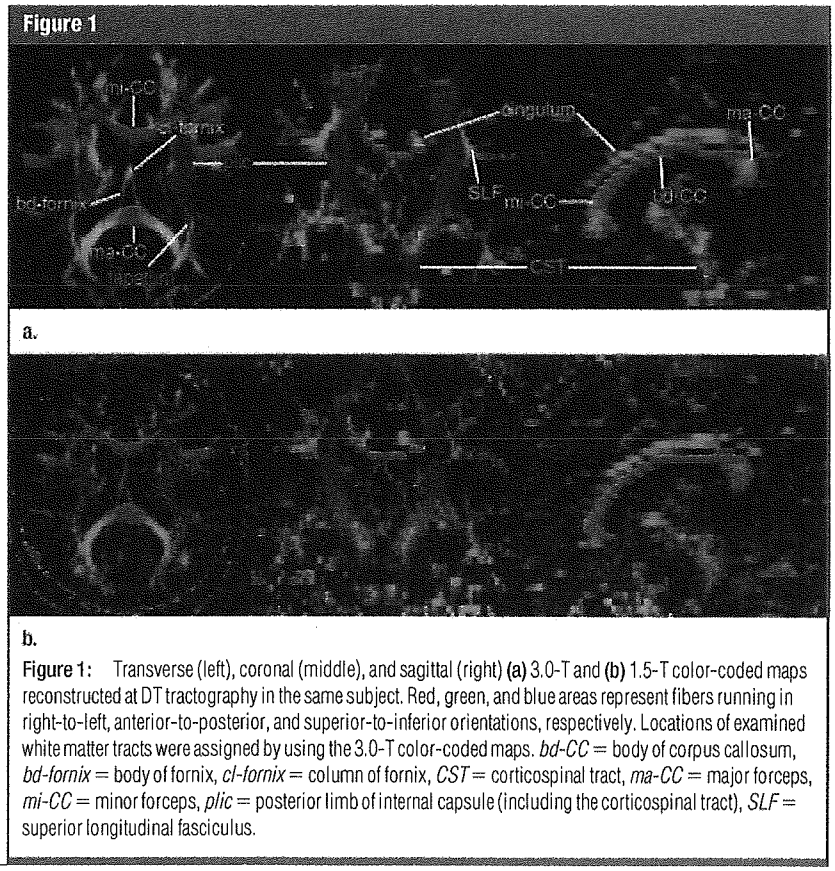

Figure 1: Transverse (left), coronal (middle), and sagittal (right) **(a)** 3.0-T and **(b)** 1.5-T color-coded maps reconstructed at DT tractography in the same subject. Red, green, and blue areas represent fibers running in right-to-left, anterior-to-posterior, and superior-to-inferior orientations, respectively. Locations of examined white matter tracts were assigned by using the 3.0-T color-coded maps. *bd-CC* = body of corpus callosum, *bd-fornix* = body of fornix, *cl-fornix* = column of fornix, *CST* = corticospinal tract, *ma-CC* = major forceps, *mi-CC* = minor forceps, *plic* = posterior limb of internal capsule (including the corticospinal tract), *SLF* = superior longitudinal fasciculus.

Figure 2

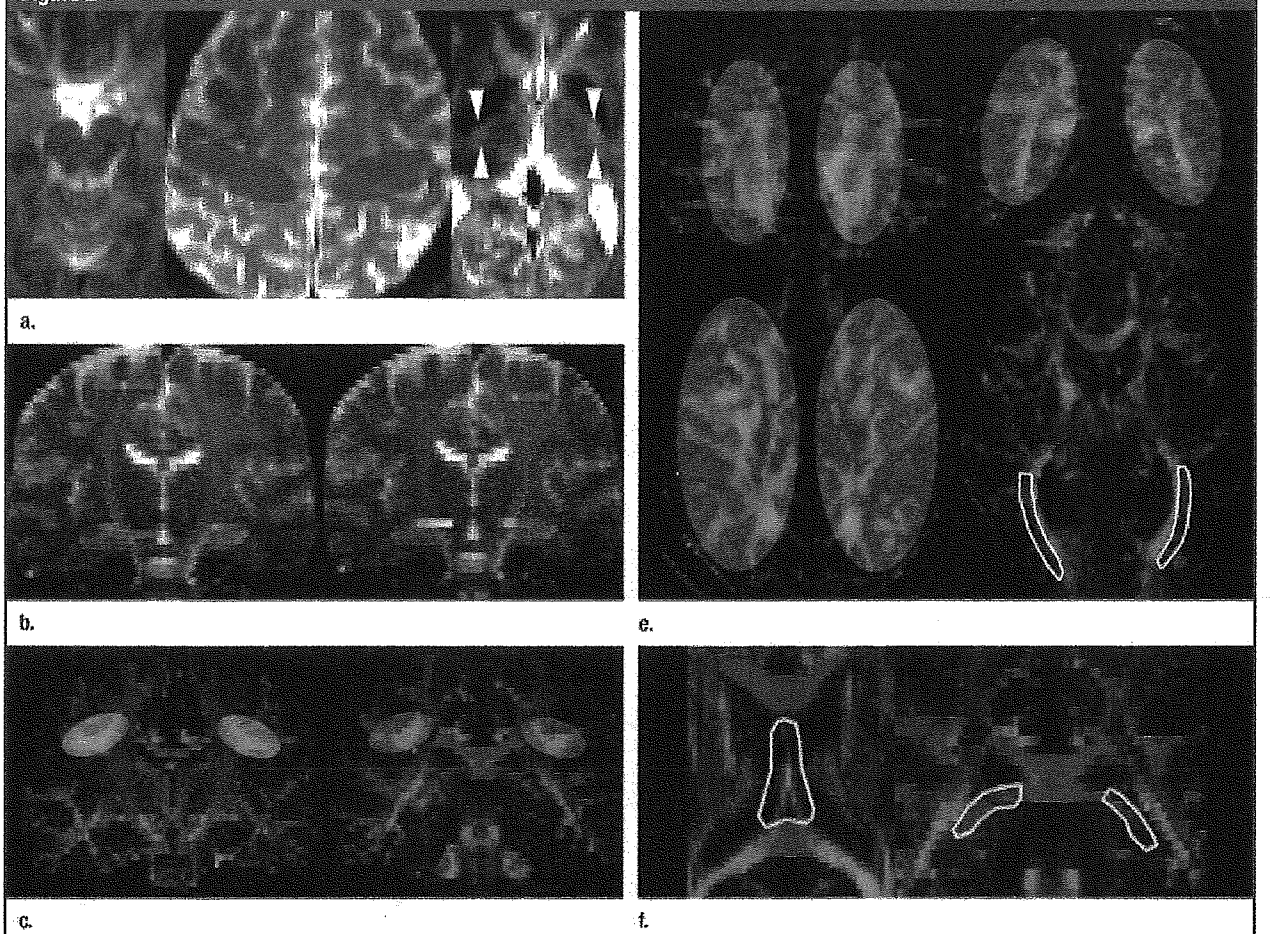

Figure 2: ROI operations used to reconstruct four tracts on 3.0-T MR images ($b = 0$ sec/mm^2, 5200/79). **(a)** Transverse images at bilateral cerebral peduncles (right), precentral gyri (middle), and internal capsule (left) show ROIs in red. Corticospinal tract is area of prolonged T2 relaxation at posterolateral aspect of internal capsule (arrowheads). **(b)** Coronal images of corticospinal tracts (red) reconstructed with cut operation. Only fibers between the ROIs (blue) were reconstructed for the right and left sides separately. **(c)** Coronal color-coded maps with ROIs (white ellipses). Anterior (left) and posterior (right) ROIs contain superior longitudinal fasciculus (green area lateral to corona radiata). **(d)** Primary ROI placed in corpus callosum on sagittal color-coded map. Vertical (coronal planes) and horizontal (transverse planes) white lines indicate section locations of secondary ROIs: anterior coronal section for minor forceps, posterior coronal for major forceps, superior transverse for body of corpus callosum, and inferior transverse for tapetum. **(e)** Transverse color-coded maps show secondary ROIs for corpus callosum: anterior ROIs for minor forceps (top left), posterior ROIs for major forceps (top right), superior ROIs for body of corpus callosum (bottom left), and inferior ROIs (white outlines) for tapetum (bottom right). **(f)** Transverse (left) and coronal (right) color-coded maps show ROIs (white outlines) for fornix. Primary (superior) ROI was placed at body of fornix (left); secondary (posterior) ROIs, at crura of fornices bilaterally (right).

losal fibers, referred to as major forceps, the ROI was placed posterior to the splenium of the corpus callosum. Callosal body fibers were reconstructed by placing the ROI at the centrum semiovale in the transverse plane superior to the body of the corpus callosum. For reconstruction of the temporal interhemispheric connection fibers, referred to as tapetum, ROIs were placed bilaterally in the temporal deep white matter, lateral to the trigon of the lateral ventricles. These four fibers (ie, minor forceps, major forceps, callosal body fibers, and tapetum) were combined to delineate the entire corpus callosum.

Limbic fibers through the fornix were reconstructed by placing one primary ROI and two secondary ROIs. The primary ROI was placed in the body of the fornix, and the secondary ROIs

Figure 3

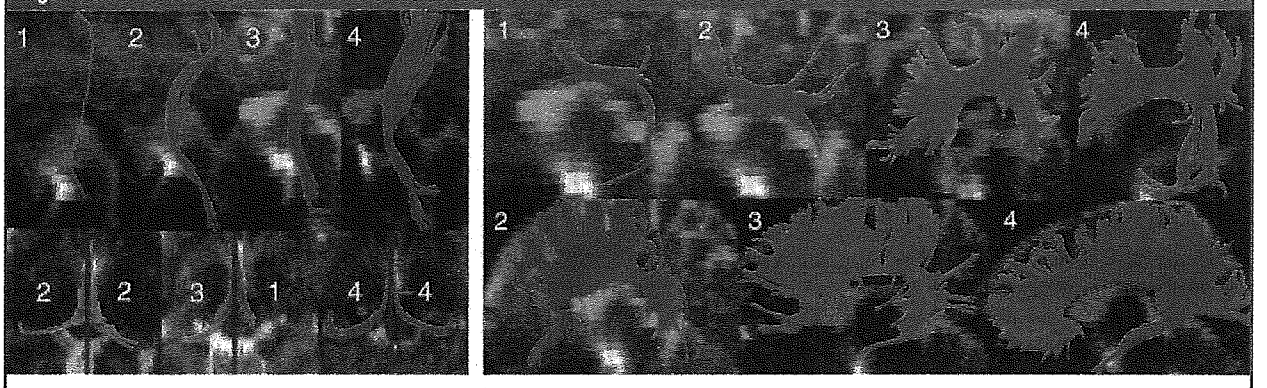

a. b.

Figure 3: Scoring (scores *1–4*) for fiber tract depiction at tractography. Red areas represent the depicted tracts. **(a)** Top: Corticospinal tractographic image superimposed on sagittal non–diffusion-weighted images (5200/79) viewed from left side. Grades *1* and *2* were assigned at 1.5-T imaging, and grades *3* and *4* were assigned at 3.0-T imaging. Bottom: Fornix tractographic image obtained at 3.0 T superimposed on transverse non–diffusion-weighted images (5200/79). Blue lines separate right and left fornix tractographic images. **(b)** Superior longitudinal fasciculus tractographic image (top) and corpus callosum tractographic image (bottom) superimposed on sagittal non–diffusion-weighted images (5200/79) viewed from left side. For superior longitudinal fasciculus tractography (top), grades 1 and 2 were assigned at 1.5-T imaging, and grades 3 and 4 were assigned at 3.0-T imaging. For corpus callosum tractography, grade 2 was assigned at 1.5 T imaging, and grades 3 and 4 were assigned at 3.0-T imaging. In no subject was grade 1 assigned at corpus callosum tractography.

were placed in the crura of the right and left fornices anterolateral to the splenium of the corpus callosum (Fig 2f).

Evaluation of Tractography

The tractographic depiction of fiber tracts was graded on three-dimensional volume views and in three orthogonal two-dimensional planes by two neuroradiologists (T.O., with 2 years of experience performing tractography; Y.M., with 3 years of experience performing tractography and 19 years of experience as a neuroradiologist). Grading was performed on the basis of the following three criteria: the fiber tract volume, the anatomic distribution of the tract, and the presence or absence of the tract at the expected location. The readers were blinded to the magnetic field strength used (1.5 or 3.0 T). After performing independent interpretations, the two readers resolved any score discrepancies by consensus to establish final scores.

One score was derived from one tractographic examination—not from the pair of ROIs used to perform reconstructing tractography. The scores assigned at fiber tractography were as follows: 4 meant excellent—that is, the depicted fiber tract accurately matched the known anatomic distribution, and there was a sufficient volume of fibers; 3 meant adequate for diagnosis—that is, imaging errors such as image distortion and tract propagation error were minor, so the image was still adequate for use as a diagnostic tool; 2 meant fair—that is, moderate imaging errors or moderate tract volume loss markedly reduced imaging quality; 1 meant poor—that is, there were major imaging errors and/or tract volume loss, and the readers were unable to interpret the course or shape of the tract; and 0 meant no tract visualization.

At corticospinal tract tractography, anatomically accurately depicted tracts were defined as those passing through the lateral segment of the cerebral peduncle, the posterior limb of the internal capsule, and the precentral gyrus. At superior longitudinal fasciculus tractography, fibers connecting the frontal and parietal lobes (ie, long association fibers) and fibers connecting the frontal and temporal lobes (ie, arcuate fibers) were considered. Anatomically accurate results for the superior longitudinal fasciculus were defined as good visualization of both the long association fibers and the arcuate fibers. At corpus callosum tractography, anatomically accurate results were defined as good visualization of the four different subsegments. At limbic tractography, the depiction of fibers connecting the column, body, and crus of the fornix was considered to represent anatomically accurate results. At tractography, the depicted superior longitudinal fasciculus, corpus callosum, and fornix are each composed of several subsegments of fiber bundles, and all subsegments were integrated to establish a single final score for each tractographic examination. The scoring of tractographic images is illustrated in Figure 3.

Tractographic depictions of the corticospinal tract, superior longitudinal fasciculus, and fornix on the right and left sides were assessed independently. At corpus callosum tractography, the right and left sides were assessed together, because callosal fiber connects the right and left hemispheres.

Reconstructed tract fibers were counted by using the DtiStudio software. The numbers of fibers depicted at tractography of the corticospinal tract and the superior longitudinal fasciculus in the right and left hemispheres were counted separately. The right and left fibers were not counted separately at tractography of the corpus callosum and

the fornix, because right- and left-hemisphere limbic fibers were difficult to differentiate at the column of the fornix, which was visualized as a single fiber bundle.

Although the diffusion characteristics of the normal brain are somewhat asymmetric, corticospinal tract tractography in healthy subjects reportedly reveals minimal asymmetry (17,29). To assess the reliability of corticospinal tract tractography in healthy subjects, lateral asymmetry was evaluated on the basis of the numbers of right- and left-hemisphere fibers at tractography of the corticospinal tract. For this purpose, the "cut" operation was performed by using DtiStudio software. With the cut operation, only the fiber coordinates between the two ROIs are reconstructed (Fig 2b). The conventional two-ROI approach involves the use of three corticospinal tract regions at tractography: the areas below the cerebral peduncle, between the two ROIs, and above the precentral gyrus. These three regions have very different properties. In the region between the two ROIs, tracking results do not branch and are more robust against noise. This approach is particularly useful for quantitative analysis.

The index of asymmetry (AI) between the right *(R)* and left *(L)* corticospinal tracts in each subject at tractography was calculated as the absolute difference in fiber numbers between the two sides, divided by the mean of the two sides, as modified from a previously described method (14): $AI = L - R / [(L + R)/2]$. Lateral asymmetry analysis of superior longitudinal fasciculus tractography was not performed, because the superior longitudinal fasciculus comprises numerous long and short connecting fibers and lateral asymmetry is commonly observed in healthy subjects (6,29).

Statistical Analyses

Differences between 3.0- and 1.5-T DT imaging were calculated in terms of the following features: *(a)* depiction scores for right and left corticospinal tract tractography, right and left superior longitudinal fasciculus tractography, corpus callosum tractography, and right and left fornix tractography; *(b)* numbers of fibers depicted at right and left tractography of the corticospinal tract, right and left tractography of the superior longitudinal fasciculus, corpus callosum tractography, and fornix tractography; and *(c)* asymmetry index at corticospinal tract tractography. Statistical

Figure 4

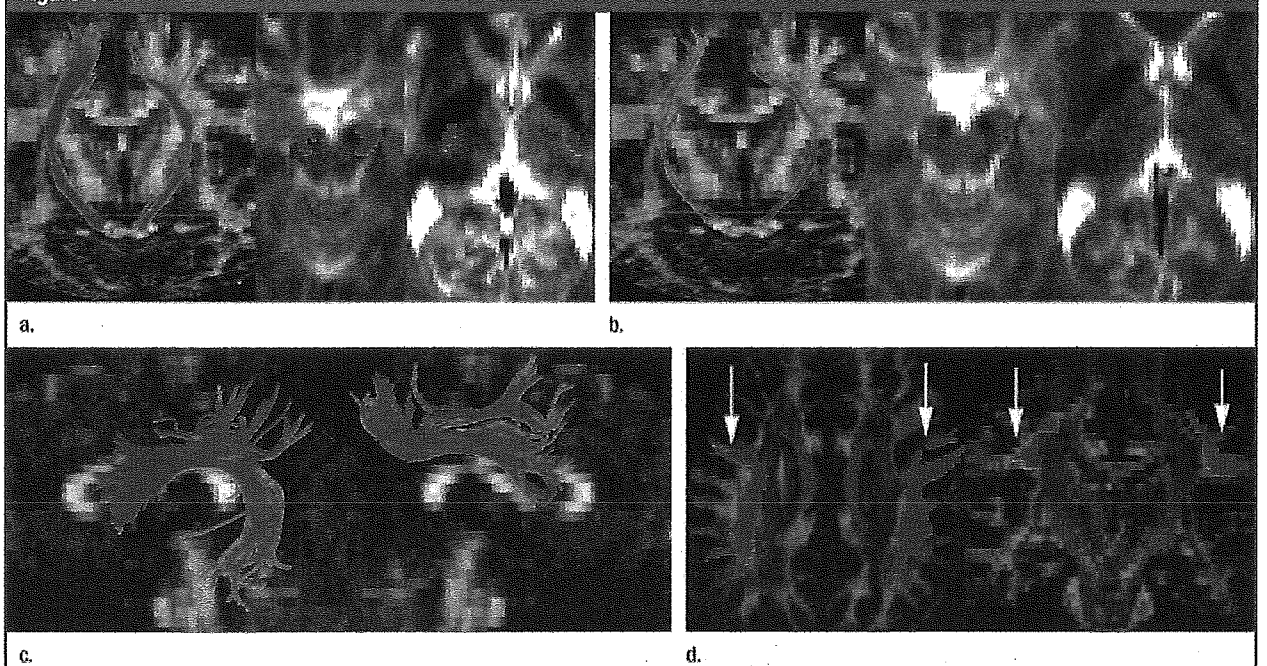

Figure 4: Fiber tractographic results. **(a, b)** Left: Three-dimensional reconstruction of corticospinal tract (red) in the same subject at **(a)** 3.0-T and **(b)** 1.5-T tractography, with use of transverse and coronal fractional anisotropy images. Middle and right: Transverse non–diffusion-weighted images with two-dimensional overlays of tractographic images at the sections of the cerebral peduncles (middle) and internal capsule (right) bilaterally. The voxels where the depicted corticospinal tract penetrates the transverse planes are shaded red. At 1.5-T corticospinal tract tractography **(b)**, although the proper anatomic distribution is depicted, the tract volume is lower than that at 3.0 T. **(c)** Three-dimensional reconstruction of superior longitudinal fasciculus (red) on sagittal fractional anisotropy map at 3.0-T tractography in a different subject. At tractography in this subject, the shapes and distributions of the right and left superior longitudinal fasciculi differed. Although tractography of the left superior longitudinal fasciculus depicted arcuate fibers toward the temporal lobe, tractography of the right superior longitudinal fasciculus depicted no arcuate fibers. The cortico-cortical long connection fibers between the frontal and parietal lobes, however, were thicker on the right side than on the left side. **(d)** Tractographic image of superior longitudinal fasciculus (red, arrows) overlaid on 3.0-T transverse (left) and coronal (right) color-coded maps obtained in the subject described in **c** *(Fig 4 continues).*

analysis was based on the consensus scores for each tract in each subject derived by the two neuroradiologists. The Wilcoxon signed rank test was applied by using JMP, version 5.1, software (SAS Institute, Cary, NC). For all statistical analyses, $P < .05$ was considered to be indicative of a significant difference.

Results

Fiber Tract Visualization

DT imaging at both 3.0 and 1.5 T was successfully performed in all 30 subjects. The corticospinal tract was visualized at 3.0 and 1.5 T (Fig 4a, 4b) in all subjects. At superior longitudinal fasciculus tractography, long association fibers were visualized in all subjects at 3.0 and 1.5 T. Right arcuate fibers were visualized in 22 subjects (73%) at 3.0 T and in 20 subjects (67%) at 1.5 T, whereas left arcuate fibers were identified in 29 subjects (97%) at 3.0 and 1.5 T (Fig 4c, 4d).

All four subsegments of the corpus callosum were successfully visualized at 3.0 and 1.5 T (Fig 4e) in every subject. The body and column of the fornix were visualized at 3.0 and 1.5 T in every subject. The right crus of the fornix was visualized in 21 subjects (70%) at 3.0 T and in 18 subjects (60%) at 1.5 T. The left crus of the fornix was visualized in 27 subjects (90%) at 3.0 T and in 25 subjects (83%) at 1.5 T (Fig 4f). One subject was incidentally found to have cavum septum pellucidum and cavum vergae. The right and left columns of the fornix were visualized separately in this subject (Fig 4g).

All tractographic results were included in the analysis of tract depiction scores and numbers of depicted tract fibers. All tractographic results for the corticospinal tract were included for asymmetry analysis. With regard to the 420 depiction scores (30 subjects times seven tracts times two readers), there were discrepancies between the two independent readers regarding 152 scores (36%). The two readers discussed the discrepancy and established a final consensus score in each case. The depicted fiber tracts and the depiction scores are listed in Table 1.

Statistical Analyses

For tractography of the corticospinal tract, both right- and left-hemisphere depiction scores ($P < .001$) and numbers of tract fibers (right, $P = .008$; left, $P < .001$) were significantly higher at 3.0 T than at 1.5 T. The asymmetry index at corticospinal tract tractography was significantly lower at 3 T ($P < .001$). For tractography of the right su-

Figure 4

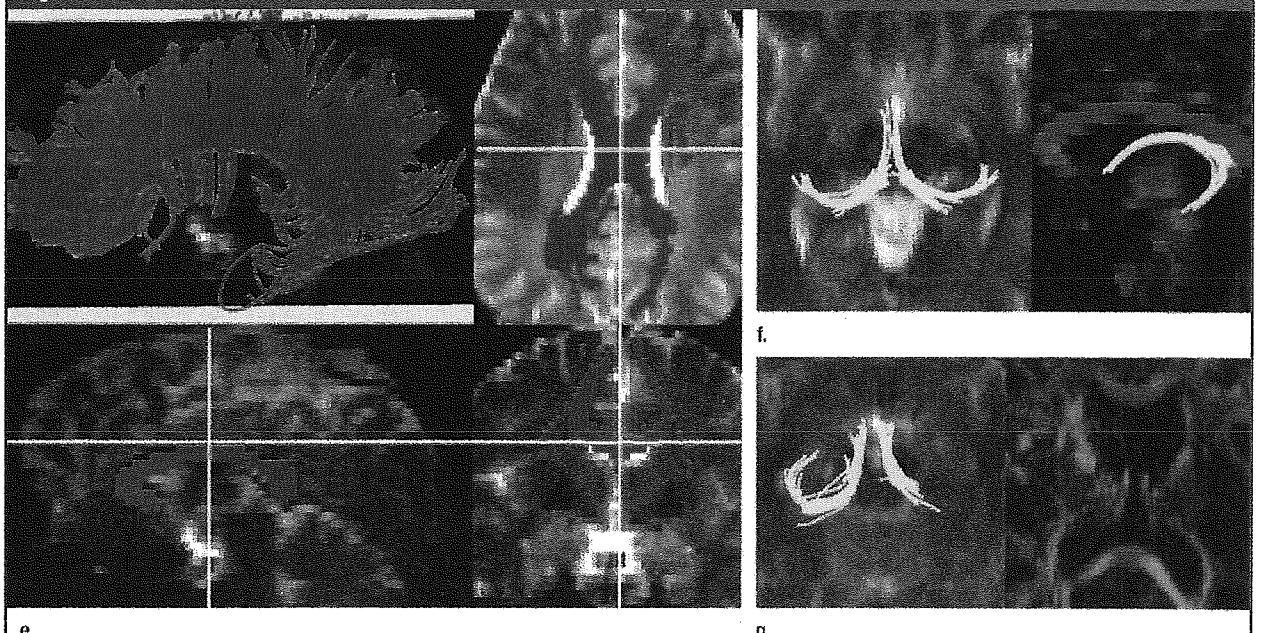

Figure 4 *(continued)*: **(e)** Three-dimensional 3.0-T tractographic reconstruction of corpus callosum (red) on sagittal non–diffusion-weighted image (5200/79) (top left) and on overlay in three orthogonal planes (top right, bottom left, and bottom right). Various kinds of transcallosal connection fibers are depicted. The center indicated by the intersecting of the vertical and horizontal lines on the three orthogonal images (top right, bottom left, and bottom right) indicate the same location. **(f)** Three-dimensional 3.0-T tractographic reconstruction of fornix (yellow) on transverse non–diffusion-weighted image (5200/79) (left) and sagittal color-coded map viewed from left (right). **(g)** Three-dimensional 3.0-T tractographic reconstruction of fornix (yellow) on transverse non–diffusion-weighted image (5200/79) (left) and transverse color-coded map (right) obtained in a subject with cavum septum pellucidum and cavum vergae. The bodies and columns of the fornices on the right and left sides were visualized separately.

perior longitudinal fasciculus, depiction scores (P = .005) and numbers of tract fibers (P = .001) were significantly higher at 3.0 T than at 1.5 T. Depiction scores for tractography of the left superior longitudinal fasciculus did not differ significantly between 3.0- and 1.5-T DT imaging. For tractography of the left superior longitudinal fasciculus, the numbers of tract fibers were significantly higher at 3.0 T than at 1.5 T (P = .02). For corpus callosum tractography, depiction scores were significantly higher at 3.0 T than at 1.5 T (P = .01), although the numbers of tract fibers did not differ significantly. Scores for depiction of the right fornix (P = .04) and numbers of fornix tract fibers bilaterally (P = .02) were significantly higher at 3.0 T than at 1.5 T, although scores for depiction of the left fornix were not significantly different. These results are summarized in Table 2.

Table 1

Depiction Scores Assigned at Fiber Tractography

Tract and Score	3.0-T Tractography	1.5-T Tractography
Right corticospinal tract		
0	0	0
1	0	2
2	1	8
3	6	13
4	23	7
Left corticospinal tract		
0	0	0
1	0	6
2	1	9
3	6	10
4	23	5
Right superior longitudinal fasciculus		
0	0	0
1	1	3
2	10	11
3	6	9
4	13	7
Left superior longitudinal fasciculus		
0	0	0
1	1	0
2	3	3
3	14	17
4	12	10
Corpus callosum		
0	0	0
1	0	0
2	2	6
3	9	14
4	19	10
Right fornix		
0	0	0
1	10	11
2	8	16
3	11	3
4	1	0
Left fornix		
0	0	0
1	3	4
2	14	17
3	12	9
4	1	0

Note.—Data are numbers of subjects with the given depiction score. Scores were determined in consensus between two readers.

Discussion

In recent studies, investigators have reported on intraindividual comparisons between 3.0- and 1.5-T DT imaging performed for functional MR imaging based on blood oxygen level–dependent contrast (30), intracranial time-of-flight MR angiography (31), supraaortic contrast material–enhanced MR angiography (32), and high-spatial-resolution inner ear imaging (33). These studies revealed the clinical feasibility of and the better visualization that is achievable at 3.0-T imaging compared with these features at 1.5-T imaging. DT imaging also reportedly yields a higher signal-to-noise ratio at 3.0 T, suggesting the possibility that it renders higher spatial resolution without enhanced noise-related errors (22,34).

Parallel imaging techniques involve the use of multiple receiver coil elements for spatial information encoding and gradient encoding and, owing to shortened echo train lengths, have been shown to markedly reduce the number of echo-planar imaging–related artifacts. The potential of parallel imaging for DT imaging has been demonstrated at both 1.5 and 3.0 T (21,22). Naganawa et al (23) challenged the optimization of 3.0-T DT fiber tractography performed with parallel imaging and found that DT imaging data on brain fiber tracking in healthy subjects can be acquired within a very short imaging time (<2 minutes). Nagae-Poetscher et al (24) performed high-spatial-resolution DT imaging of the brainstem at 3.0 T with parallel imaging and visualized various brainstem structures, including deep cerebellar nuclei, some cranial nerves, and white matter tracts.

To our knowledge, our study is the first in which the findings of 3.0- and

1.5-T DT fiber tractography, both performed with parallel imaging, were compared in a relatively large number of subjects. Improved image quality was observed at 3.0-T tractography of the corticospinal tract.

More complex results were observed at tractography of the superior longitudinal fasciculus. Although the right superior longitudinal fasciculus was visualized significantly better at 3.0 T, the depiction score for left superior longitudinal fasciculus tractography did not differ significantly between 3.0 and 1.5 T. The numbers of tract fibers depicted at 3.0 T were significantly higher than the numbers of fibers depicted at 1.0 T. We speculated that the reason for this was as follows: According to fiber dissection study findings, the corticospinal tract is a long projection fiber bundle with a well-established anatomic distribution (35). Most fibers in the corticospinal tract run parallel through the posterior limb of the internal capsule, without sharp turning angles or directional diversity.

Conversely, both the superior longitudinal fasciculus and the corpus callosum consist of groups of fiber bundles that comprise association or commissural fibers of varying lengths and directions. The superior longitudinal fasciculus contains arcuate fibers that turn sharply toward the temporal lobe. This sharp turning angle may surpass the tracking terminate threshold, and tracking does not extend to reach the temporal lobe. Temporal fibers are susceptible to image distortion at the middle cranial fossa and temporal bone, where the air-tissue interface induces magnet susceptibility artifacts. Thus, we propose that temporal arcuate fibers are more affected by image distortion than are long association fibers. In the present study, left arcuate fibers were visualized in a larger number of subjects than were right arcuate fibers at both 3.0 and 1.5 T. Such asymmetry of the arcuate fibers at tractography may be due to image distortion or the known lateral asymmetry of temporal fibers (36), and, thus, differences between 3.0- and 1.5-T DT imaging may be underestimated on the left side.

Table 2

Analyses of Tract Depiction Scores and Numbers of Tract Fibers

Tract	Difference in Depiction Score*	*P* Value†	Difference in No. of Tract Fibers*	*P* Value‡
Right corticospinal tract§	0.87 ± 0.15	<.001	27 ± 12	.008
Left corticospinal tract	1.32 ± 0.21	<.001	70 ± 9.2	<.001
Right superior longitudinal fasciculus	0.52 ± 0.16	.005	192 ± 57	.001
Left superior longitudinal fasciculus	0.03 ± 0.14	NS	65 ± 34	.02
Corpus callosum	0.34 ± 0.12	.01	220 ± 149	NS
Right fornix	0.35 ± 0.16	.04	...	...
Left fornix	0.19 ± 0.15	NS	...	...
Left and right fornices	...	...	14 ± 5.5	.02

Note.—NS = not significant.

* Data are mean difference values ± standard deviations.

† *P* values for difference in depiction scores at 1.5- versus 3.0-T tractography.

‡ *P* values for difference in numbers of tract fibers at 1.5- versus 3.0-T tractography.

§ The mean asymmetry index for the corticospinal tract was 0.47 ± 0.11 (standard deviation), and the difference in corticospinal tract asymmetry index at 1.5- versus 3.0-T tractography was significant ($P < .001$).

For corpus callosum tractography, tract depiction scores were better at 3.0 T than at 1.5 T but the numbers of tract fibers did not differ significantly. At corpus callosum tractography, the crossing-fiber problem of unidirectional tracking models (37) may contribute to the discrepancies observed between depiction scores and tract fiber numbers. Corpus callosum tractography is susceptible to the crossing-fiber problem at the centrum semiovale. In this area, a small number of callosal fibers intersect a large number of corticospinal tract fibers. Thus, corpus callosum tractography might reveal a smaller number of fibers than the appropriate fiber trajectory owing to limitations related to the crossing-fiber problem, and differences between 3.0- and 1.5-T imaging may be underestimated.

The statistical methods used may have been responsible for the differences in results obtained at analyses of the depiction scores and the numbers of tract fibers. Although mean differences in the numbers of depicted fibers between 3.0- and 1.5-T imaging were as large as 220, no significant difference was noted. This was probably because of the relatively large numbers of depicted fibers (mean numbers: 3784 at 3.0 T and 3565 at 1.5 T). Low statistical power also may have contributed to this lack of a significant difference.

Depiction scores for right fornix tractography were significantly better at 3.0 T than at 1.5 T, but no significant differences were noted for the left fornix. The numbers of tract fibers depicted at 3.0-T fornix tractography were significantly higher than the numbers depicted at 1.5-T tractography. This result was probably due to the relatively lower volume of limbic fibers compared with the volumes of other fiber bundles. Our DT imaging voxel size was 1.7 × 1.7 × 3.0 mm. The body and crus of the fornix are composed of narrow fiber bundles—they are smaller in diameter than a single voxel—so partial volume-averaging artifacts would have had a greater effect in this region than in the other fiber tracts.

The present study had some limitations. First, the imaging parameters for 3.0-T imaging were not optimized to achieve the best DT image quality. For the most part, we used identical imaging parameters to perform 3.0- and 1.5-T imaging for comparisons so that features other than magnetic field strength would be equivalent. However, differences in T1 and T2* interfere with the equal conditions between 3.0- and 1.5-T imaging. A DT imaging sequence optimized for 1.5-T imaging is not the optimal sequence for 3.0-T imaging. The differences in bandwidth between 3.0- and 1.5-T imaging also may have biased

our results. We tried to keep other acquisition parameters equivalent between 3.0- and 1.5-T imaging, but the bandwidth was higher at 3.0 T. Higher bandwidth results in a reduced signal-to-noise ratio and reduced image distortion. DT imaging at 3.0 T yields a higher signal-to-noise ratio and causes greater magnet susceptibility artifacts owing to the higher static magnetic field strength. We adjusted parameters so that we could use a bandwidth of 1502 Hz per pixel for 3.0-T imaging, which is up to 50% higher than the bandwidth used for 1.5-T imaging. Further optimization of 3.0-T imaging to improve the quality of DT images may be required in the future.

Second, the development of imaging methods to reduce the effects of the crossing-fiber problem, such as high angular DT imaging with high *b* values (38) and diffusion-spectrum imaging (36), is progressing. Other fiber-tracking methods, such as probabilistic tractography to estimate the probability of fiber connections through the data field (39), also are advancing. These advanced methods will affect the results of both 3.0-T and 1.5-T tractography.

In conclusion, DT tractography at 3.0 T enables improved visualization of the corticospinal tract compared with DT tractography at 1.5 T, and 3.0-T tractography of the superior longitudinal fasciculus, corpus callosum, and fornix has some advantages over 1.5-T tractography. Advances in efficient MR sequences are needed to improve the image quality and reliability of 3.0-T DT tractography.

References

1. Basser PJ, Mattiello J, LeBihan D. MR diffusion tensor spectroscopy and imaging. Biophys J 1994;66:259–267.
2. Beaulieu C. The basis of anisotropic water diffusion in the nervous system: a technical review. NMR Biomed 2002;15:435–455.
3. Chenevert TL, Brunberg JA, Pipe JG. Anisotropic diffusion in human white matter: demonstration with MR techniques in vivo. Radiology 1990;177:401–405.
4. Pierpaoli C, Jezzard P, Basser PJ, Barnett A, Di Chiro G. Diffusion tensor MR imaging of the human brain. Radiology 1996;201:637–648.
5. Basser PJ, Pajevic S, Pierpaoli C, Duda J, Aldroubi A. In vivo fiber tractography using DT-MRI data. Magn Reson Med 2000;44:625–632.
6. Mori S, van Zijl PC. Fiber tracking: principles and strategies—a technical review. NMR Biomed 2002;15:468–480.
7. Masutani Y, Aoki S, Abe O, Hayashi N, Otomo K. MR diffusion tensor imaging: recent advance and new techniques for diffusion tensor visualization. Eur J Radiol 2003;46:53–66.
8. Dong Q, Welsh RC, Chenevert TL, et al. Clinical applications of diffusion tensor imaging. J Magn Reson Imaging 2004;19:6–18.
9. Stieltjes B, Kaufmann WE, van Zijl PC, et al. Diffusion tensor imaging and axonal tracking in the human brainstem. Neuroimage 2001;14:723–735.
10. Wakana S, Jiang H, Nagae-Poetscher LM, van Zijl PC, Mori S. Fiber tract–based atlas of human white matter anatomy. Radiology 2004;230:77–87.
11. Clark CA, Barrick TR, Murphy MM, Bell BA. White matter fiber tracking in patients with space-occupying lesions of the brain: a new technique for neurosurgical planning? Neuroimage 2003;20:1601–1608.
12. Yamada K, Kizu O, Mori S, et al. Brain fiber tracking with clinically feasible diffusion-tensor MR imaging: initial experience. Radiology 2003;227:295–301.
13. Huisman TA, Schwamm LH, Schaefer PW, et al. Diffusion tensor imaging as potential biomarker of white matter injury in diffuse axonal injury. AJNR Am J Neuroradiol 2004;25:370–376.
14. Glenn OA, Henry RG, Berman JI, et al. DTI-based three-dimensional tractography detects differences in the pyramidal tracts of infants and children with congenital hemiparesis. J Magn Reson Imaging 2003;18:641–648.
15. Kunimatsu A, Aoki S, Masutani Y, Abe O, Mori H, Ohtomo K. Three-dimensional white matter tractography by diffusion tensor imaging in ischaemic stroke involving the corticospinal tract. Neuroradiology 2003;45:532–535.
16. Tanenbaum LN. 3-T MR imaging: ready for clinical practice [letter]. AJNR Am J Neuroradiol 2004;25:1626–1627.
17. Zhai G, Lin W, Wilber KP, Gerig G, Gilmore JH. Comparisons of regional white matter diffusion in healthy neonates and adults performed with a 3.0-T head-only MR imaging unit. Radiology 2003;229:673–681.
18. Sodickson DK, Manning WJ. Simultaneous acquisition of spatial harmonics (SMASH): fast imaging with radiofrequency coil arrays. Magn Reson Med 1997;38:591–603.
19. Pruessmann KP, Weiger M, Scheidegger MB, Boesiger P. SENSE: sensitivity encoding for fast MRI. Magn Reson Med 1999;42:952–962.
20. Griswold MA, Jakob PM, Heidemann RM, et al. Generalized autocalibrating partially parallel acquisitions (GRAPPA). Magn Reson Med 2002;47:1202–1210.
21. van den Brink JS, Watanabe Y, Kuhl CK, et al. Implications of SENSE MR in routine clinical practice. Eur J Radiol 2003;46:3–27.
22. Jaermann T, Crelier G, Pruessmann KP, et al. SENSE-DTI at 3 T. Magn Reson Med 2004;51:230–236.
23. Naganawa S, Koshikawa T, Kawai H, et al. Optimization of diffusion-tensor MR imaging data acquisition parameters for brain fiber tracking using parallel imaging at 3 T. Eur Radiol 2004;14:234–238.
24. Nagae-Poetscher LM, Jiang H, Wakana S, Golay X, van Zijl PC, Mori S. High-resolution diffusion tensor imaging of the brain stem at 3 T. AJNR Am J Neuroradiol 2004;25:1325–1330.
25. Bastin ME, Armitage PA. On the use of water phantom images to calibrate and correct eddy current induced artefacts in MR diffusion tensor imaging. Magn Reson Imaging 2000;18:681–687.
26. Pajevic S, Pierpaoli C. Color schemes to represent the orientation of anisotropic tissues from diffusion tensor data: application to white matter fiber tract mapping in the human brain. Magn Reson Med 1999;42:526–540.
27. Naidich TP, Valavanis AG, Kubik S. Anatomic relationships along the low-middle convexity. I. Normal specimens and magnetic resonance imaging. Neurosurgery 1995;36:517–532.
28. Mori S, Kaufmann WE, Davatzikos C, et al. Imaging cortical association tracts in the human brain using diffusion-tensor-based axonal tracking. Magn Reson Med 2002;47:215–223.
29. Lazar M, Field AS, Lee J, et al. Lateral asymmetry of superior longitudinal fasciculus: a white matter tractography study (abstr). In: Proceedings of the 12th Meeting of the International Society for Magnetic Resonance in Medicine. Berkeley, Calif: International Society for Magnetic Resonance in Medicine, 2004; 1290.

30. Fera F, Yongbi MN, van Gelderen P, Frank JA, Mattay VS, Duyn JH. EPI-BOLD fMRI of human motor cortex at 1.5 T and 3.0 T: sensitivity dependence on echo time and acquisition bandwidth. J Magn Reson Imaging 2004;19:19–26.

31. Willinek WA, Born M, Simon B, et al. Time-of-flight MR angiography: comparison of 3.0-T imaging and 1.5-T imaging—initial experience. Radiology 2003;229:913–920.

32. Willinek WA GJ, von Falkenhausen M, et al. 3.0T contrast-enhanced, submillimeter MRA of the supraaortic arteries: does the signal gain at high field strength allow to replace the phased array coil by the quadrature body coil? (abstr). In: Proceedings of the 12th Meeting of the International Society for Magnetic Resonance in Medicine. Berkeley, Calif: International Society for Magnetic Resonance in Medicine, 2004; 1523.

33. Graf H, Schick F, Claussen CD, Seemann MD. MR visualization of the inner ear structures: comparison of 1.5 Tesla and 3 Tesla images. Rofo 2004;176:17–20.

34. Hunsche S, Moseley ME, Stoeter P, Hedehus M. Diffusion-tensor MR imaging at 1.5 and 3.0 T: initial observations. Radiology 2001; 221:550–556.

35. Yagishita A, Nakano I, Oda M, Hirano A. Location of the corticospinal tract in the internal capsule at MR imaging. Radiology 1994;191:455–460.

36. Lin CP, Wedeen VJ, Chen JH, Yao C, Tseng WY. Validation of diffusion spectrum magnetic resonance imaging with manganese-enhanced rat optic tracts and ex vivo phantoms. Neuroimage 2003;19:482–495.

37. Wiegell MR, Larsson HB, Wedeen VJ. Fiber crossing in human brain depicted with diffusion tensor MR imaging. Radiology 2000; 217:897–903.

38. Tuch DS, Reese TG, Wiegell MR, Makris N, Belliveau JW, Wedeen VJ. High angular resolution diffusion imaging reveals intravoxel white matter fiber heterogeneity. Magn Reson Med 2002;48:577–582.

39. Behrens TE, Woolrich MW, Jenkinson M, et al. Characterization and propagation of uncertainty in diffusion-weighted MR imaging. Magn Reson Med 2003;50:1077–1088.

Ken-ichiro Kikuta, M.D., Ph.D.
Department of Neurosurgery,
Kyoto University Graduate School
of Medicine,
Kyoto, Japan

Yasushi Takagi, M.D., Ph.D.
Department of Neurosurgery,
Kyoto University Graduate School
of Medicine,
Kyoto, Japan

Kazuhiko Nozaki, M.D., Ph.D.
Department of Neurosurgery,
Kyoto University Graduate School
of Medicine,
Kyoto, Japan

Takashi Hanakawa, M.D., Ph.D.
Human Brain Research Center,
Kyoto University School of Medicine,
Kyoto, Japan

Tsutomu Okada, M.D.
Department of Diagnostic Imaging
and Nuclear Medicine,
Kyoto University
School of Medicine,
Kyoto, Japan

Yukio Miki, M.D., Ph.D.
Department of Diagnostic Imaging
and Nuclear Medicine,
Kyoto University School of Medicine,
Kyoto, Japan

Yasutaka Fushimi, M.D.
Department of Diagnostic Imaging
and Nuclear Medicine,
Kyoto University School of Medicine,
Kyoto, Japan

Hidenao Fukuyama, M.D., Ph.D.
Human Brain Research Center,
Kyoto University School of Medicine,
Kyoto, Japan

Nobuo Hashimoto, M.D., Ph.D.
Department of Neurosurgery,
Kyoto University Graduate School
of Medicine,
Kyoto, Japan

Reprint requests:
Ken-ichiro Kikuta, M.D., Ph.D,
Department of Neurosurgery,
Kyoto University
Graduate School of Medicine,
54 Kawaharacho, Shogoin,
Sakyo-ku, Kyoto
606-8507, Japan.
Email: kikuta@kuhp.kyoto-u.ac.jp

Received, May 18, 2005.
Accepted, September 7, 2005.

EARLY EXPERIENCE WITH 3-T MAGNETIC RESONANCE TRACTOGRAPHY IN THE SURGERY OF CEREBRAL ARTERIOVENOUS MALFORMATIONS IN AND AROUND THE VISUAL PATHWAY

OBJECTIVE: To evaluate of the role of magnetic resonance (MR) tractography on the optic radiation with a 3-T MR unit in the surgery of cerebral arteriovenous malformation (AVM) in and around the visual pathway.

METHODS: Of the 322 patients with cerebral AVMs admitted to our clinic between 1978 and 2005, a study of MR tractography was made on 29 patients. Ten of those patients had AVMs in and around the visual pathway and were included in this study. There were two men and eight women ranging in age from 15 to 64 years (mean age, 34.5 ± 14.8 yr). All of the patients underwent 3-T tractography of optic radiation (OR) and neuro-ophthalmologic evaluation. Four of the 10 patients underwent surgical resection of the AVM. A postoperative 3-T MR study and a neuro-ophthalmologic evaluation was performed 1 month after surgery in most patients.

RESULTS: The preoperative patients for whom tractography demonstrated a continuous bundle of OR from the medial temporal region to the primary visual cortex had minimal or no visual field loss, whereas the patients for whom the tractography did not show a continuous bundle of OR had significant visual loss. The patients for whom tractography in the postoperative study demonstrated a bundle of OR experienced no postoperative deterioration of the visual field loss, whereas the patients for whom tractography did not demonstrate a bundle of OR exhibited significant visual field loss.

CONCLUSION: This technique is thought to be useful in confirming the integrity of and localizing deviated tract and in evaluating the surgical risk, especially for nonhemorrhagic AVMs in and around the visual pathways, taking some limitations of this method into consideration.

KEY WORDS: Arteriovenous malformation, Diffusion tensor tractography, Optic radiation, Surgical indication, 3-Tesla magnetic resonance imaging

Neurosurgery 58:331-337, 2006 DOI: 10.1227/01.NEU.0000195017.82776.90 www.neurosurgery-online.com

In palliative treatment of arteriovenous malformations (AVMs), there is an inverse increase in the risk of bleeding (12). Thus, in the surgery of AVMs, complete resection of the nidus is always required even if other intraaxial lesions do not allow complete resection to avoid postoperative deficits. Surgical indication for AVMs usually is determined according to the risk of postoperative deficits when complete resection is accomplished. Surgical indication for AVMs is usually determined according to the risk of postoperative deficits when complete resection is accomplished.

Recent advances in magnetic resonance (MR) technology have made it possible to describe major neural tracts in the white matter by diffusion tensor tractography (2, 4, 13, 14, 21), including the visual pathways in the occipitotemporal connections (10). Diffusion corresponds to the random motion of water molecules. Although the tissue exhibits the property of anisotropy in the region where

diffusion of water varies significantly with direction, it shows low anisotropy (expressed as isotropic) in the regions where diffusion is similar in all directions (11, 20). Anisotropy can be quantified by one of several indices, including fractional anisotropy (FA). These indices are derived from a full description in the region of interest (the diffusion tensor) obtained by measuring changes in the nuclear MR signal with diffusion sensitization along at least six noncollinear directions. In an axonal cylinder, water diffusion is faster along the axon than across it, probably because of the presence of structures, including the axonal membrane and the neurofilamentary cytoskeleton, which behave as barriers to diffusion. Because fiber tracts are composed of collections of similarly oriented axons that generally exhibit high anisotropy values, FA reflects the integrity of fiber tracts. Diffusion within each voxel can be described by three mutually perpendicular eigenvectors, whose magnitude is given by three corresponding eigenvalues. The eigenvalues are the three principal diffusion coefficients measured along the three eigenvector directions that define the local fiber frame of references for that voxel. The direction of fiber is thus given by the eigenvector of the largest eigenvalue of the diffusion tensor (11, 20).

We reported that a 3-T MR unit can describe most of neural tracts more clearly than a 1.5-T unit (8, 15). Tractography of the four neural tracts (corticospinal tract, superior longitudinal fasciculus, corpus callosum, and fornix) described by a 3-T unit was compared with that by a 1.5-T unit in the degree of inspective recognition by the observers, in the quantitative number of fiber bundles, and in the right-left asymmetry of the number of bundles. The 3-T unit showed significant better performance in all three aspects in describing the corticospinal tract, and in at least one of the three aspects in describing other three neural tracts (15). This study provides the results of early experiences using 3-T MR tractography in the surgery of cerebral AVMs in and around the visual pathway.

PATIENTS AND METHODS

Patients

Of the 322 patients with AVMs admitted to our clinic between 1978 and 2005, 29 underwent 3-T MR tractography. Ten of those patients had AVMs in and around the visual pathway and were included in this study. There were two men and eight women ranging in age from 15 to 64 years (mean age, 34.5 ± 14.8 yr). Three patients experienced hemorrhagic onset. Four had migraine-like episodes and four exhibited some visual field loss. The location of the AVMs was the occipital pole in three patients, the medial portion of the occipital lobe in one, the lateral portion of the occipital lobe in two, the posterior portion of the temporal lobe in three, and the thalamus in one. The Spetzler-Martin grade of the AVMs was I in two patients, II in three patients, III in three patients, and IV in two patients. The characteristics of the patients are shown in *Figure 1*. Four of the 10 patients (Patients 1–4) underwent surgical treatment. Surgical resection alone was performed in Patients 1, 2, and 4, and surgery after embolization was performed in Patients 3. The characteristics of the patients who had surgical treatment are shown in *Figure 2*. Complete obliteration of the lesion was confirmed in all surgical cases by postoperative angiography.

Neuro-ophthalmologic Evaluation

A Goldmann perimetry was performed in all 10 patients to assess visual field loss. Postoperative examinations were performed once 1 month after surgery in two patients, twice in one patient 1 week and 1 month after surgery, and twice in one patient 1 month and 5 months after surgery. Visual field defects of the patients were classified into five grades (normal, incomplete quadrantanopia, complete quadrantanopia, incomplete hemianopia, complete hemianopia) according to the amount of loss reported previously (6, 7) (*Figs. 1* and *2*).

Imaging Methods

All patients were studied before surgery with the same 3-T MR scanner (Magnetom Trio; Siemens, Erlangen, Germany). In four surgical patients, a postoperative MR study was carried out once 1 month after surgery in three patients and twice in one patient 1 month and 5 months after surgery. Images were obtained with axial T2-weighted turbo spin echo sequences (TR/TE = 8400/108 ms; flip angle, 150°; matrix, 512 × 448; field of view, 22 cm; 40 slices; slice thickness, 2.3 mm; interslice gap, 0.7 mm and twice averaging) and with axial T1-weighted three-dimensional magnetization-prepared rapid acquisition gradient-echo (MPRAGE) sequences (TR/TE/TI = 2000/4.4/990 ms; flip angle, 8°; matrix, 256 × 240; field of view, 24 cm; 208 slices; slice thickness, 1 mm, no interslice gap and single averaging). At the same time, thin-section diffusion-tensor imaging was performed. The diffusion-tensor imaging acquisition time was 4 minutes and 24 seconds. A single-shot spin echo echo-planar imaging technique was used (repetition time/echo time = 5300/79 ms) with a motion-probing gradient in 12 orientations, a b value of 700 seconds/mm^2, and four times averaging. The generalized autocalibrating partially parallel acquisitions algorithm was applied for parallel imaging, with a reduction factor of 2 and 24 additional autocalibrating phase-encoding steps in the center of k space. The reconstructed images had a 128 × 128 matrix. A total of 40 sections were obtained with a thickness of 3 mm without interslice gaps. The imaging field center for T2-weighted images, MPRAGE, and diffusion tensor imaging were adjusted to the same location.

Data Processing

We transferred the diffusion-tensor imaging data to an offline workstation for data analysis. DTI studio software version 2.03 (H. Jiang, S. Mori; Department of Radiology, Johns Hopkins University) was used for tensor calculations (11, 20). After calculating the six independent elements of the 3 × 3 tensor and diagonalization, three eigenvalues and eigenvectors were

case	1	2	3	4	5	6	7	8	9	10
age	38	27	29	28	15	37	55	64	25	27
gender	F	F	F	F	F	F	F	M	M	F
onset	headache, scintillating scottoma	hemorrhage	headache, scintillating scottoma	hemorrhage	headache, scintillating scottoma	hemorrhage	headache, scintillating scottoma	incidental	headache	vertigo
size (cm)	2	2	4	4	4	4	4	2	4	5
side	L	R	R	R	R	R	R	R	R	L
location	occipital, medial	temporal, posterior	occpital, lateral	temporal, posterior	occipital, lateral	thalamus	occipital pole	occipital pole	temporal, posterior	occipital pole and thalamus
S-M grade	I	I	II	III	III	IV	IV	II	II	III
visual field loss	incomplete homonimous quadrantanopia	complete homonimous hemianopia	none	none	none	complete homonimous quadrantanopia	none	none	none	complete homonimous hemianopia
3-tesla MR tractgraphy of OR	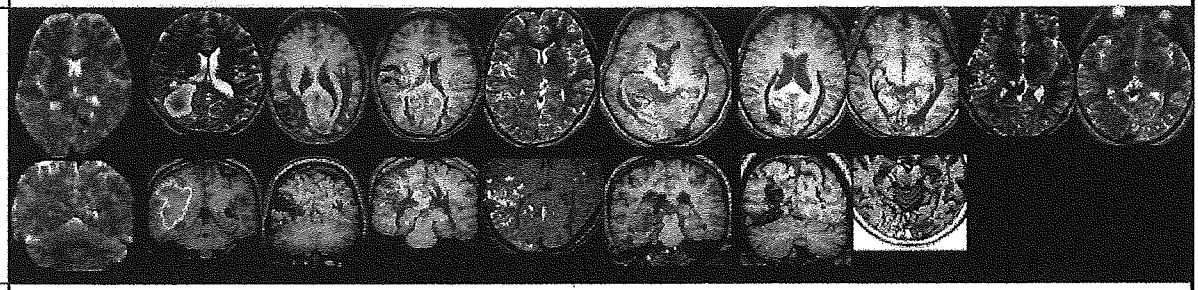									
State of OR	Grade II: running just besides the nidus	Grade V: disrupted	Grade II: running just besides the nidus	Grade I: running completely apart from the nidus	Grade III: passing through the nidus	Grade IV: fairly described on the tractgraphy	Grade III: passing through the nidus	Grade II: running just besides the nidus	Grade I: running completely apart from the nidus	Grade V: disrupted

FIGURE 1. *Diagram summarizing the 10 patients with AVMs in and around the optic radiation who underwent a 3-T MR study. It gives the age, sex, type of onset, side, location, Spetzler-Martin grade of the lesion, surgical indication, amount of preoperative visual field defect, MR tractography of OR, and interpretation of the findings of tractography.*

obtained. The eigenvector associated with the largest eigenvalue was assumed to represent the intravoxel fiber orientation. An FA map and a directional color-coded map were synthesized. Starting from a particular region of interest, one can follow the direction of the principal eigenvector, thus following the corresponding fiber. Translation of eigenvectors into neuronal trajectories was achieved by a technique known as the fiber assignment by continuous tracking method, which was initially described by Mori et al. (11). The procedure for mapping neural connections is performed by designating two regions of interest in the three-dimensional space on DTI studio software. Region of interest segmentation was performed by one author (TO). The region of interest placement starts at the lateral geniculate ganglion in bilateral mesial temporal region on coronal b = 0 images. Then a secondary region of interest was added at the bilateral occipital lobe on the coronal images. The optic radiation (OR) was identified as a green color area abutting the trigone of lateral ventricle in the temporo-occipital deep white matter on a coronal color-coded map (17, 20). The secondary regions of interest were placed at the area as described on a coronal color-coded map. This method was useful when the AVMs were situated close to the primary visual cortex and the primary visual cortex was difficult to identify based on the sulcal patterns. Tracking was terminated when it reached a pixel with low FA (<0.2) or a predetermined trajectory curvature between two contiguous vectors (inner product, <0.75). Fiber tracts that passed through both regions of interest were designed to be the final tract of interest. The traced fiber tracts in this study included OR and temporal part of inferior occipito-frontal fasciculi. There are the arcuate fibers and the fibers with downward projection from the splenium of corpus callosum (tapetum) that courses near the OR/inferior occipitofrontal fasciculus (IOFF) complex in the temporal lobe. These fibers are the structures localized lateral to the OR/IOFF complex and along with the z axis of MRI scanner, whereas the OR/IOFF complex exists mainly along with the *y* axis. Therefore, their presentation and orientation apparently can be discriminated from those of the OR/IOFF complex on the FA map and can be deleted selectively on the software (7, 15). A typical tract reconstruction by using a two-region of interest method required approximately 1 minute by using a 3.2-GHz Pentium IV workstation (Dell, Austin, TX). The entire data postprocessing time for ORs on both hemispheres took approximately 10

case	age	gender	intervention	Preopeartive study		Postoperative status		
				state of the OR	visual field loss	state of the OR (timing of the study)		visual field loss (timing of the study)
1	38	F	surgery	running just lateral to the nidus	incomplete quadrantanopia	preserved (1 mo. after surgery)	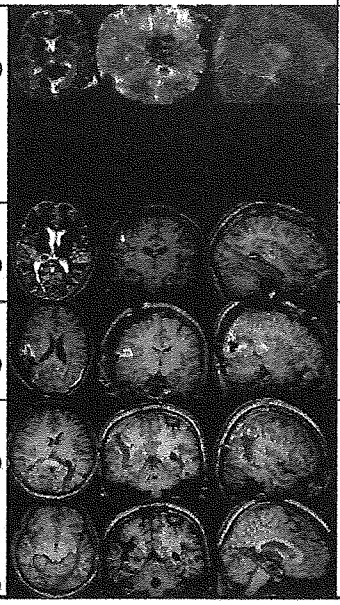	complete quadrantanopia (1 wk. after surgery) incomplete quadrantanopia (1 mo. after surgery)
2	28	F	surgery	running apart from the nidus	no defect	preserved (1mo. after surgery)		no defect (1mo. after surgery)
3	29	F	surgery after embolization	running just inferomedial to the nidus	no defect	disrupted (1mo. after surgery)		incomplete hemianopia (1mo. after surgery)
4	27	F	surgery	disrupted	conplete hemianopia	remained disrupted (1mo. after surgery) appeared to be running just benieth the nidus (5 mo. after surgery)		conplete hemianopia (1mo. after surgery) Incomplete quadrantanpoia (5 mo. after surgery)

FIGURE 2. *Diagram summarizing four patients who received surgical treatment for AVMs. It provides the age, sex, type of onset, amount of preoperative and postoperative visual field defect, postoperative MR tractography of OR, and interpretation of preoperative and postoperative tractography.*

to 15 minutes after completion of the examination, including the data transfer to the off-line workstation.

Evaluation of the State of OR on Tractography and the Geometrical Relationship between the Nidus and the OR

When the OR could be described as a continuous bundle, the geometrical relationship between the nidus and the OR was evaluated by fusing the images of tractography and those of MPRAGE or T2-weighted images. The field center for T2-weighted image, MPRAGE, and diffusion tensor imaging were adjusted, and a fusion image was obtained using DTI studio by simple overlay. Our diffusion tensor imaging obtained with a Siemens MR scanner had low eddy current geometric distortion (1), and the parallel imaging technique also contributed to the lower magnetic susceptibility related artifact. A simple overlay is enough for creating fusion images with the same field center. OR tractography was classified into five grades as described: Grade I, the OR was running completely apart from the nidus; Grade II, the OR was running just beside the nidus; Grade III, the OR was passing through the nidus or projecting into the nidus. When the OR could not be described clearly, the state of OR description was graded as follows: Grade IV, the OR was fairly described on the tractography; Grade V, the OR cannot be described completely (disrupted).

RESULTS

Relationship between the Findings of Tractography and the Amount of Visual Field Loss before Surgery

The OR could be described as a continuous bundle on preoperative tractography in seven patients. The OR coursed apart from the nidus in two patients and just beside the nidus in three patients and passed through the nidus in two patients. In the remaining three patients, the OR was fairly described on the tractography in one patient and was disrupted by the hematoma or the huge nidus in two patients. The first seven patients had no or minimal visual field loss at presentation, whereas the remaining three patients exhibited severe visual field loss at presentation. As for the four patients with migraine-like episodes at presentation, the OR coursed just beside the nidus or passed through the nidus.

Relationship between the Findings of Tractography and the Amount of Visual Field Loss after Surgery

Among the four patients who underwent surgical treatment, the OR was preserved in the postoperative study 1 month after surgery in two patients (Patients 1, 2) (*Fig. 2*). The two patients exhibited no deterioration of visual field loss 1 month after surgery. In Patient 1, transient worsening of visual field loss occurred within 1 week of surgery, but the deficits

were improved to preoperative status by 1 month after surgery. In Patient 3, a large part of the occipital lobe had to be removed because of intraoperative normal perfusion pressure breakthrough. The OR could not be described on the postoperative study 1 month after surgery, and deterioration of visual field loss occurred after surgery. In Patient 4, the OR was disrupted by a hematoma both in the preoperative study and in the study 1 month after surgery. However, the OR seemed to be described in the study at 5 months after surgery in accordance with the shrinkage of the hematoma. The amount of visual field loss of the patient was unchanged 1 month after surgery, but was much reduced 5 months after surgery (*Fig. 2*).

Preoperative and Postoperative FA Maps and Quantitative FA Values in the Representative Patients

In Patient 1, ORs on both sides in the preoperative (*Fig. 3A*) and the postoperative OR tractography (*Fig. 3B*) were well visualized on the three-dimensional view of OR tractography, the two-dimensional view of OR tractography overlaid on axial FA map, and on axial MPRAGE images. Postoperative FA values along the tract did not differ from preoperative ones. In Patient 3, preoperative and postoperative left OR tractography were well visualized, but postoperative right OR tractography seemed to be damaged (*Fig. 4*). Patient 3 exhibited lower FA values in postoperative tractography than preoperative tractography in the affected hemisphere.

DISCUSSION

In the surgery of cerebral AVMs, complete obliteration is always required because palliative treatment inversely increases the risk of bleeding (12). We previously reported that a dissection technique with minimal coagulation that preserves the intranidal venous drainage is important for avoiding postoperative neurological deterioration (3). In addition, one of the most important factors of a favorable surgical outcome is that surgical indication is determined according to the risk of postoperative neurological aggravation when complete resection is accomplished.

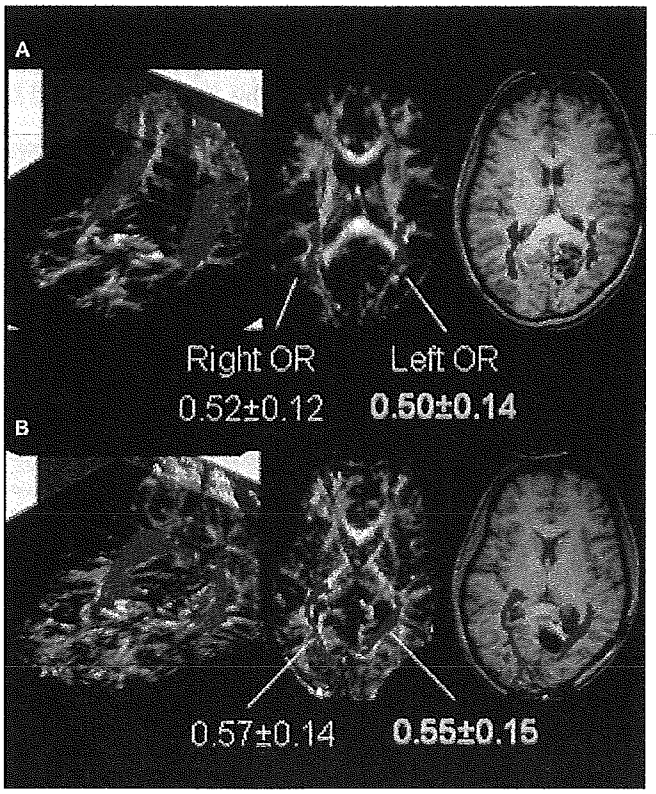

FIGURE 3. A, *preoperative and* (B) *postoperative images of Patient 1, who had a left occipital AVM:* (left) *Three-dimensional view of OR tractography,* (middle) *two-dimensional view of OR tractography overlaid on axial FA map, and* (right) *axial MPRAGE images. Both preoperative and postoperative OR tractography are well visualized on both sides, and postoperative FA values (mean ± standard deviation) along the tract on the affected side do not differ from preoperative values.*

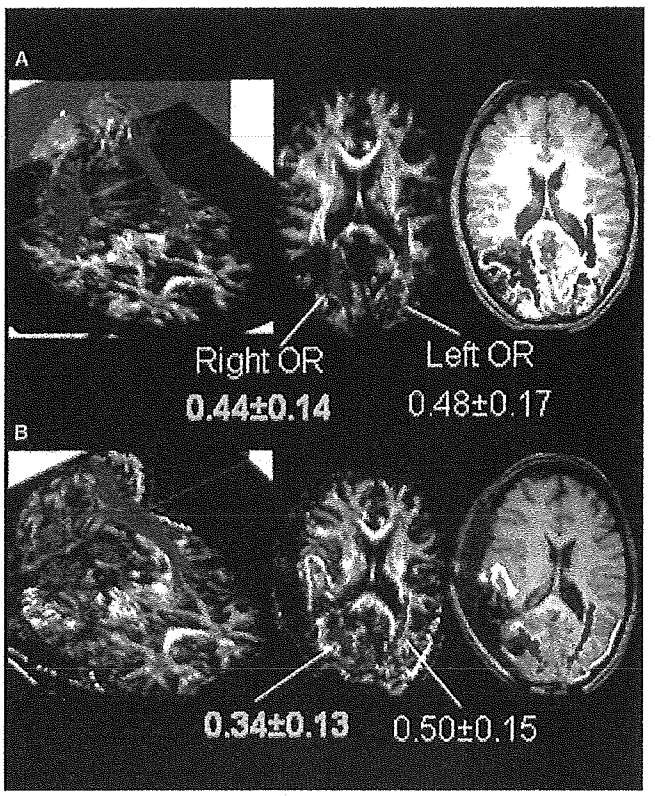

FIGURE 4. A, *preoperative and* (B) *postoperative images of Patient 3, who had a right occipital AVM:* (left) *Three-dimensional view of OR tractography,* (middle) *two-dimensional view of OR tractography overlaid on axial FA map, and* (right) *axial MPRAGE images. Preoperative and postoperative left OR tractography are well visualized, but the postoperative right OR exhibits lower FA values in postoperative tractography than preoperative tractography in the affected hemisphere.*

MR tractography by diffusion tensor imaging has realized visualization of the major neural tracts in the white matter both in physiological and pathological conditions (2, 4, 10, 13, 14, 19). Prognosis of motor function in the patients with lenticulostriate infarcts was related to the geometrical relationship between the lesion and motor fibers on the tractography (13). MR tractography visualized sensorimotor fibers in the patients with AVMs situated near sensorimotor cortices (19). Use of a neuronavigation system combined with the tractography of the corticospinal tract in tumor surgery also was reported (4, 14).

In this study, we used a 3-T MR unit in the evaluation of the surgical risk of AVMs situated near the OR, because a 3-T unit can describe most of neural tracts more clearly than 1.5-T units (8, 15). The patients exhibited minimal or no visual field loss when the OR could be described as a continuous bundle. The patient for which the OR was disrupted or fairly described on the tractography exhibited severe visual field loss. The findings of postoperative tractography also corresponded with the amount of visual field loss. These findings suggest that estimation of the state of OR and evaluation of the geometrical relationship between the nidus and the OR are useful for determining the surgical risk of AVMs in and around the visual pathways. Currently, we exclude patients who exhibit minimal or no preoperative visual field loss from the surgical indication of AVMs in and around the visual pathways when the OR is described as a bundle passing through or projecting to the nidus.

Postoperative transient worsening of visual field loss was observed in two patients. In one patient, transient worsening occurred 1 week after surgery. The OR could be described at 1 month after surgery and visual field loss of the patient recovered to the preoperative status. In this patient, transient worsening might have been caused by mechanical injury by surgical manipulation or by transient change of regional blood flow around the OR. In three of the four patients who underwent surgery, the amount of visual field loss correlated to the state of OR in the study 1 month after surgery. Tractography of the OR also may be useful to predict the prognosis of postoperative visual field deficits and the optimal time for the study to estimate the state of OR at 1 month after surgery.

Functional translocation sometimes occurs in the brain of patients with cerebral AVMs (5, 9, 19). In this series, there were two patients (Patients 2 and 8) exhibiting no visual field loss such that the course of the OR was deviated by the nidus. The OR passed through the nidus in two patients (Patients 5 and 7) who also exhibited visual field loss. Although further investigation is necessary, tractography of the OR may indicate whether the functions for vision remain in the neural tissue within the nidus. That is critical in determining surgical indication of AVMs.

There are three limitations in this study. Visual loss of the patients with disruption of the OR by hematoma on the tractography at presentation seemed to improve in accordance with the shrinking of the hematoma. However, description of the OR was less in all patients with hematoma (Patients 2, 4, and 6) than in patients without hematoma. These observations show not only that the description of the OR in the tractography corresponded to the visual functions, but also suggest the possibility that the tractography in our method has less ability to describe the tract under existence of hematoma. Our study potentially has the technical concerns of a single-shot technique regarding possible susceptibility artifacts from the hematoma that may cause signal intensity drop-off around the nidus on the source diffusion tensor images. Our method should be feasible for most nonhemorrhagic AVMs, and evaluation of the tractography should be performed at least after the hematoma has been completely absorbed in those with hematoma.

Some investigators may recommend higher performance of the tractography in a higher number of directions instead of 12 directions in describing the tracts with severely curved or tortuous projection, such as motor fibers of hands in the corticospinal tract and Meyer's loop in the visual pathway. Because we performed the tractography in 12 directions in this study, it was possible that a part of the OR with a severely curved course (Meyer's loop) could not be estimated well. Although we have preliminary data indicating that description of the OR by tractography in 40 and in 81 directions did not significantly differ from by the tractography in 12 directions, this is another limitation of this study that should be examined in the future.

The third limitation is that the grading of the state of OR was determined according to visualization of the tract. It is very difficult to be certain if the tract is really destroyed or disrupted, especially when the OR cannot be visualized on the tractography (Grade V). There is a report of tumor cases suggesting that disruption of the corticospinal tract (CST) on the tractography does not always mean the functional disruption of the tract and that location of CST probed by motor evoked potential often was apart from the corresponding site where tractography is indicated (14). However, we recently reported that location of the CST indicated by intraoperative motor evoked potential corresponded to the site where the tractography is indicated in most patients of our series, mainly patients with nonneoplastic lesions (16). There is a possibility that tractography in patients with tumor cannot reflect the function of the tract so correctly as in patients with AVMs because histopathological change, such as perifocal edema or infiltration of the tumor, often exists in the white matter of tumor patients. Quantitative FA values have a potential to enable the functional evaluation of the tract (18), and an FA value of approximately 0.20 has been reported to be the optimal trackability threshold of the CST (6), which was the same value of the threshold used in our study. This issue will be resolved in the future by the accumulation of data regarding correlation between the function of the tract and the quantitative FA values.

CONCLUSION

In summary, this technique is thought to be useful in confirming the integrity and to localize deviated tract and in

evaluating surgical risk, especially in patients with nonhemorrhagic AVMs in and around the visual pathways, taking some limitations of this method into consideration.

REFERENCES

1. Bastin ME, Armitage PA: On the use of water phantom images to calibrate and correct eddy current induced artefacts in MR diffusion tensor imaging. **Magn Reson Imaging** 18:681–687, 2000.
2. Cabanis EA, Iba-Zizen MT, Nguyen TH, Bellinger L, Stievenart JL, Yoshida M: The visual pathways, from anatomical MRI to physiological with (f)MRI and tractography with diffusion tensor MRI (DTMRI). **Bull Acad Natl Med** 188:1153–1169, 2004.
3. Hashimoto N: Microsurgery for cerebral arteriovenous malformations: A dissection technique and its theoretical implications. **Neurosurgery** 48:1278–1260, 2001.
4. Kinoshita M, Yamada K, Hashimoto N, Kato A, Izumoto S, Baba T: Fiber-tracking does not accurately estimate size of fiber bundle in pathological condition: Initial neurosurgical experience using neuronavigation and subcortical white matter stimulation. **Neuroimage** 25:424–429, 2005.
5. Kombos T, Pietila T, Kern BC, Kopetsch O, Brock M: Demonstration of cerebral plasticity by intra-operative neurophysiological monitoring: Report of an uncommon case. **Acta Neurochir (Wien)** 141:885–889, 1999.
6. Kunimatsu A, Aoki S, Masutani Y, Abe O, Hayashi N, Mori H: The optimal trackability threshold of fractional anisotropy for diffusion tensor tractography of the corticospinal tract. **Magn Reson Med Sci** 3:11–7, 2004.
7. Kupersmith MJ, Vargas ME, Yashar A, Madrid MRN, Nelson K, Seton A: Occipital arteriovenous malformations: Visual disturbances and presentation. **Neurology** 46:953–957, 1996.
8. Larsson EM, Stahlberg F: 3 Tesla magnetic resonance imaging of the brain. Better morphological and functional images with higher magnetic field strength [in Swedish]. **Lakartidningen** 102:460–463, 2005.
9. Lazar RM, Marshall RS, Pile-Spellman J, Hacein-Bey L, Young WL, Mohr JP: Anterior translocation of language in patients with left cerebral arteriovenous malformation. **Neurology** 49:802–808, 1997.
10. Marco C, Derek KJ, Rosario D, Dominic H: Occipito-temporal connections in the human brain. **Brain** 126:2093–2107, 2003.
11. Mori S, van Zijl PC: Fiber tracking: principles and strategies—a technical review. **NMR Biomed** 15:468–480, 2002.
12. Miyamoto S, Hashimoto N, Nagata I, Nozaki K, Morimoto M, Taki W: Posttreatment sequelae of palliatively treated cerebral arteriovenous malformations. **Neurosurgery** 46:589–594, 2000.
13. Nakagawa M, Nishimura T: MR tractography for the evaluation of functional recovery from lenticulostriate infarcts. **Neurology** 64:108–113, 2005.
14. Nimsky C, Ganslandt O, Hastreiter P, Wang R, Benner T, Sorensen AG: Preoperative and intraoperative diffusion tensor imaging-based fiber tracking in glioma surgery. **Neurosurgery** 56:130–137, 2005.
15. Okada T, Miki Y, Fushimi Y, Hanakawa T, Kanagaki M, Yamamoto A: Diffusion tensor fiber tractography: Intra-individual comparison of 3 T and 1.5 T. **Radiology** (in press).
16. Okada T, Mikuni N, Miki Y, Kikuta K, Urayama S, Hanakawa T: Integration of diffusion tensor tractography of the corticospinal tract using 3T with intraoperative white matter stimulation mapping: Preliminary results to validate corticospinal tract localization. **Radiology** (in press).
17. Pajevic S, Pierpaoli C: Color schemes to represent the orientation of anisotropic tissues from diffusion tensor data: Application to white matter fiber tract mapping in the human brain. **Magn Reson Med** 42:526–540, 1999.
18. Shimorry JS, Mckinstry RC, Akbudak E, Aronovitz JA, Snyder AZ, Lori NF: Quantitative diffusion-tensor anisotropy brain MR imaging: Normative human data and anatomic analysis. **Radiology** 212:770–784, 1999.
19. Turski PA, Cordes D, Mock B, Wendt G, Sorenson JA, Fitzurka-Quigley M: Basic concepts of functional MR imaging of arteriovenous malformations. **Neuroimaging Clin N Am** 8:371–381, 1998.
20. Wakana S, Jiang H, Nagae-Poetsce LM, Peter CM, van Zijl PC, Mori S: Fiber tract-based atlas of human white matter anatomy. **Radiology** 230:77–87, 2004.
21. Yamada K, Kizu O, Ito H, Kubota T, Akada W, Goto M: Tractography for arteriovenous malformations near the sensorimotor cortices. **AJNR Am J Neuroradiol** 26:598–602, 2005.

COMMENTS

This study investigates 10 patients with cerebral arteriovenous malformations (AVMs) that were intimate with the optic radiations. Three presented with hemorrhage, and four patients underwent surgical excision. Using 3-T magnetic resonance tractography, the status of the optic radiations was determined both at presentation and after surgical resection in the four patients. There was excellent correlation between the integrity of the optic radiations as imaged on the magnetic resonance studies and the status of the visual fields. Although these results are not surprising, 3-T magnetic resonance tractography may be a useful technique to predict which patients are likely to experience visual field loss after surgical resection of AVMs that are adjacent to the optic radiation or visual cortex.

Robert A. Solomon
New York, New York

Diffusion tensor imaging is a potentially valuable tool for preoperative planning, and may provide information that could be clinically important and that is virtually impossible to obtain with conventional anatomical techniques, such as T1, T2 and flair imaging. This method uses information obtained from anisotropic diffusibility of the water in the white matter tracts. Nowadays, the diffusion tensor technique is used increasingly, as it is present in most commercially available magnetic resonance scanners. This study by Kikuta et al. provides some interesting information, such as the good correlation between the integrity of the odds ratio in the tractography and the absence of important visual field defect, at least anecdotally. Other than the good correlation between what they called disrupted tract and the visual field defect, there are some technical limitations that deserve comment, for instance the magnetic field distortion in the hemorrhagic cases that could be responsible for misinterpretation of the real odds ratio status. Also, we do not know for sure if the tract is completely or only partially represented in the color-coded map. That is why the role of the diffusion tensor imaging in planning and postoperative follow-up still has to be defined. The fast technical improvement in software and hardware will certainly shorten this time and, in the near future, we will really be able to inform about the real status of the white matter tracts.

Nelson F. Ferreira
Evandro P. de Oliveira
São Paulo, Brazil

The authors have used a novel imaging technique which has proven useful in both the preoperative prediction of visual loss associated with resection of AVMs in and near the optic radiations and in the postoperative differentiation between permanent deficits and those likely to improve with time. Although their series is small, the findings are compelling. If they are confirmed by other surgeons, magnetic resonance tractography may be a very helpful addition to our evaluation armamentarium in selected patients.

Duke S. Samson
Dallas, Texas

平成１７年度委託業務報告書

健康安心プログラム
分子イメージング機器研究開発プロジェクト
悪性腫瘍等治療支援分子イメージング機器研究開発プロジェクト
悪性腫瘍等治療支援分子イメージング機器研究開発に係る
フィージビリティスタディ
報告書

株式会社島津製作所

要約

3．「近接撮像型フレキシブル分子イメージング装置の研究開発に係る
フィージビリティスタディ」（株式会社島津製作所）

超高感度と高解像度を両立させた近接型分子イメージング装置の検討を行った。医療動向、分子プローブの実用化の時期などを総合的に判断し、ガンマ線並びに光計測技術を用いた近接型の特性を最も効果的に評価できる対象として乳がんを第一の適合疾患とした。また、超高感度を維持し、ピクセル分解能を 1mm とするガンマ線検出器と診断機器の概念設計を行うことを目標とし、蛍光同時計測用検出器としての実現可能性を併せて評価した。

新方式の 4 層 3 次元放射線検出器（DOI 検出器）を試作し、超小型シンチレータ結晶の 3 次元位置が識別できることを示した。また、世界初の 8 層 DOI 検出器を試作し、DOI 技術のさらなる可能性を示した。DOI 検出器により 1mm 径の点線源が視野内で均一に画像化できることを計算機シミュレーションで確認し、DOI 検出器の近接配置により解像度と感度を飛躍的に向上できることを明らかにした。さらに、新開発のトラッキング同時計数処理法により視野外のノイズ成分を 80%以上の確率で弁別できる可能性を示した。

光の同時計測では、ガンマ線 DOI 検出器の性能を劣化させずに蛍光が同時に検出できる実験結果を示し、近赤外波長による微小な乳がんの検出可能性を計算機シミュレーションで確認した。また、近接型分子イメージング装置で要求される多チャンネル高集積アナログ ASIC を試作し、性能に全く問題がないことを確認した。

以上の評価結果はいずれも満足できるもので、本フィージビリティスタディで設定した目標仕様は達成できる見込みであり、近接型分子イメージング装置の実現の見通しが得られた。なお、途初として乳がんを対象としたが、今回開発する各要素技術は、次世代 PET-CT、PET-MR などの複合装置のキーコンポーネントとして、がんを始めとする幅広い疾患に対応が可能であり、各要素技術を確立した後の波及効果は大きいと考えられる。

目次